Shape anisotropic colloidal particle fabrication using 2-photon polymerization

Saraswat, Yug C.; Ibis, Fatma; Rossi, Laura; Sasso, Luigi; Eral, Huseyin Burak; Fanzio, Paola

DOI
10.1016/j.jcis.2019.12.035

Publication date
2020

Document Version
Final published version

Published in
Journal of Colloid and Interface Science

Journal of Colloid and Interface Science 564 (2020) 43–51

Contents lists available at ScienceDirect

Journal of Colloid and Interface Science

journal homepage: www.elsevier.com/locate/jcis

Shape anisotropic colloidal particle fabrication using 2-photon polymerization

Yug C. Saraswat [a], Fatma Ibis [a], Laura Rossi [b], Luigi Sasso [c], Huseyin Burak Eral [a,*], Paola Fanzio [c]

[a] Process & Energy Laboratory, Delft University of Technology, Leeghwaterstraat 39, 2628 CB Delft, the Netherlands
[b] Department of Chemical Engineering, Delft University of Technology, van der Maasweg 9, 2629 HZ Delft, the Netherlands
[c] University of Technology, Dep. Precision and Microsystems Engineering, Mekelweg 2, 2826 CD Delft, the Netherlands

HIGHLIGHTS

- Shape anisotropic colloidal particles produced via 2-photon polymerization.
- Particle dimension and shape can be controlled down to a minimum dimension of 1 μm.
- Experimental diffusivity of disk colloids agrees with the analytical model.
- Shape anisotropy deviates diffusivity from the model for disks of given aspect ratio.

GRAPHICAL ABSTRACT

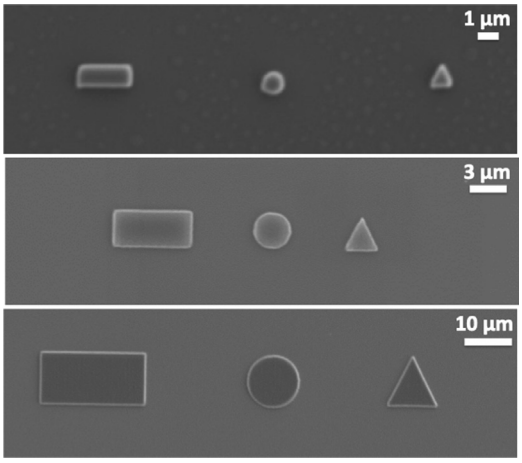

ARTICLE INFO

Article history:
Received 12 July 2019
Revised 7 December 2019
Accepted 8 December 2019
Available online 14 December 2019

Keywords:
Two-photon polymerization
Shape anisotropic colloids
Brownian motion

ABSTRACT

Hypothesis: Our ability to dictate the colloid geometry is intimately related to self-assembly. The synthesis of anisotropic colloidal particles is currently dominated by wet chemistry and lithographic techniques. The wet chemical synthesis offers limited particle geometries at bulk quantities. Lithographic techniques, on the other hand, provide precise control over the particle shape, although at lower yields. In this respect, two-photon polymerization (2PP)[1] has attracted growing attention due to its ability to automatically fabricate complex micro/nano structures with high resolution.
Experiments: We manufacture precisely designed colloids with sizes ranging from 1 μm to 10 μm with 2PP and optimize the process parameters for each dimension. Moreover, we study the shape dependent Brownian motion of these particles with video microscopy and estimate their diffusion coefficients.

* Corresponding author.
E-mail addresses: yug@yugdecor.com (Y.C. Saraswat), F.Ibis-1@tudelft.nl (F. Ibis), L.Rossi@tudelft.nl (L. Rossi), H.B.Eral@tudelft.nl (H.B. Eral).

[1] 2PP – 2 photon polymerization.

https://doi.org/10.1016/j.jcis.2019.12.035
0021-9797/

3D printing
Colloidal particles
Particle tracking
Two photon lithography

Findings: We observe that increasing the geometrical anisotropy leads to a pronounced deviation from the analytically predicted diffusion coefficient for disks with a given aspect ratio. The deviation is attributed to stronger hydrodynamic coupling with increasing anisotropy. We demonstrate, for the first time, 2PP manufacturing of colloids with tailored geometry. This study opens synthesis of colloidal building blocks to a broader audience with limited access to cleanrooms or wet-chemistry know-how.

1. Introduction

The shape of a colloidal particle plays a fundamental role in regulating its entropic interaction with other colloidal particles [1] as well as its hydrodynamic interactions [2]. Depending on the nature of these interactions, anisotropic particles can serve as simple building blocks for self-assembled structures and dictate their functionality [3,4]. Cubic crystals [5], complex polyhedra [6], degenerate crystals [7] are few examples which illustrate the importance of particle shape in forming self-assembled structures. Particle shape can facilitate particle recognition [8–10], guided particle packings [11,12] and phase transitions [13,14]. A broad variety of applications like photonics [15], biomimetics [16], diagnostics [17], drug delivery systems [10,18–21] and tissue engineering [22] can potentially benefit from the development of such building blocks.

Multiple techniques have been reported in the literature to fabricate colloidal particles with unique geometries and high production yields [23,24]. These include wet chemical methods [25–28], template assisted synthesis [29–32], controlled deformation of spherical particles [33–35], swelling and phase separation techniques [36–38], electro spraying [18] and mould stretching [39]. Apart from these techniques, considerable research has been carried out in the use of lithographic techniques such as photolithography [40,41], holographic lithography [42], interference lithography [43] and novel microfluidic processes [22,44–47] to realize complex geometries and particle morphologies. In fact, the freedom to realize complex three-dimensional (3D) geometries, high particle throughput and ease of fabrication form the desired combination for a fabrication technique.

Recently, additive manufacturing has emerged as a powerful tool for producing objects with user-defined geometry [48]. 3D printing allows fabrication of objects in a layer-by-layer fashion based on a computer-aided design[2] (CAD). The object is fabricated either by melting and depositing a thermoplastic polymer (known as fused deposition modelling) [49] or by locally curing a photopolymer using ultraviolet[3] (UV) light (called stereolithography) [50]. These are the conventionally used 3D printing techniques. However, the spatial resolution in both the techniques is too low for realizing colloidal particles.

An emerging 3D printing technology is the two photon polymerization (2PP) technique, based on the two-photon absorption (2PA)[4] process [51]. In this technique, a femto-second infrared laser is focused on a photosensitive material to cure the photopolymer and build 3D microstructures. The high resolution (lower than 200 μm) of this technique is due to the non-linear interaction of light with matter which confines the polymerization process to the focal volume (called voxel) of the laser [52]. The use of 2PP has grown constantly in the past few years in the fields of photonics [53,54], cell scaffolds and tissue engineering [55], microfluidics [56] and mechanical micro-structures [57].

In this paper, we demonstrate for the first time, that two-photon polymerization can be used for the fabrication of colloidal particles with a custom 3D shape. The printing parameters in the fabrication process were optimized to produce particles with rectangular, triangular and circular cross-sections and dimensions ranging between 1 μm and 10 μm with high fidelity. By releasing the particles in an aqueous dispersion, we measured their Brownian trajectories using video microscopy and calculated their mean squared displacement[5] (MSD). From the MSDs we calculated the in-plane diffusion coefficient for various particle geometries. We observed that the calculated diffusion coefficients for rectangular and triangular cross sections deviate from the analytically predicted diffusion coefficient for disks with a matching aspect ratio. This deviation is attributed to hydrodynamic coupling between the particle shape and the surrounding fluid. Moreover, this finding highlights the relevance of geometrical anisotropy on the diffusion coefficient of colloidal particles.

The goal of this paper is to introduce a new application of 2PP i.e. fabrication of shape anisotropic colloids. The 2PP fabricated colloidal particles may not only serve as colloidal building blocks for self-assembly but also for applications in diagnostics, biomedicine and drug delivery. Moreover, the ease of automatically producing precisely shaped 3D particles with 2PP can open new alleys of investigations in diffusive behaviour of particles with complex shapes and their self-assembly kinetics.

2. Materials and methods

2.1. Particle fabrication and imaging

2.1.1. Fabrication of colloidal particles via 2-photon polymerization

A glass coverslip (30 mm in diameter) with a thickness of 0.17 mm (±0.01 mm) was cleaned with oxygen plasma at 60 W for 1 min. A 3% solution of polyvinyl alcohol, PVA[6] (Sigma-Aldrich) in water was spin-coated at 5000 rpm for 60 s, to produce a thin film with a thickness of 120 nm (see Supplementary information). The film was then dried at room temperature overnight. (Fig. 1a). A custom design for the colloidal particles was created with Solidworks and printed via two-photon polymerization (Photonic Professional GT, Nanoscribe) on the multilayer substrate. The particles were printed in the conventional (oil immersion) mode using the IPL-780 resin (Nanoscribe) and a 63x objective **(**Fig. 1b**).** Afterwards the coverslip, with the printed structure on top of it, was immersed for 25 min in propylene glycol monomethyl ether acetate,[7] PGMEA, (≥99.5%, ReagentPlus R, Sigma-Aldrich), followed by 5 min in 2-propanol to remove the uncured resist (Fig. 1c). Then, the substrate was dried with an air gun. The particles adhere on the PVA film and can be easily stored in a dry environment (Fig. 1d). Despite the fact that acrylate chemistry is the most commonly used material, **2**PP offers flexibility in material choice as it can produce particles with any UV cross linkable chemistry including biocompatible materials for cell culture and tissue engineering.

[2] CAD – computer aided design.
[3] UV – Ultraviolet.
[4] 2PA – 2 photon absorption.
[5] MSD – mean squared displacement.
[6] PVA – polyvinyl alcohol.
[7] PGMEA - Propylene glycol monomethyl ether acetate.

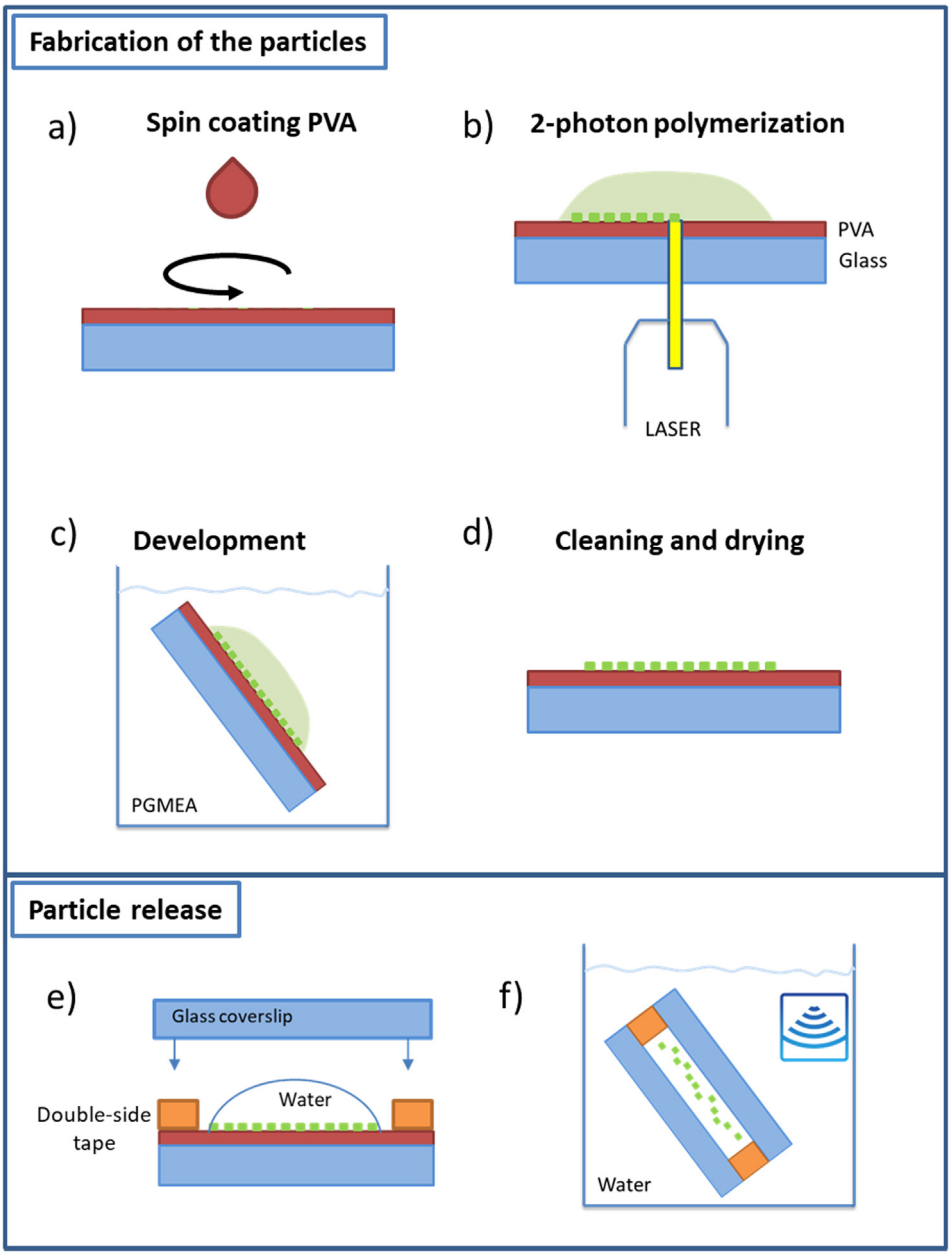

Fig. 1. Manufacturing process of 2PP colloidal particles: (a) Spin coating the sacrificial layer of PVA, (b) automated 2PP process, (c) Development of the polymerized 2PP particles, (d) Cleaning and drying of the particles, (e) Preparation of observation chamber (f) Particle release process by eroding the sacrificial layer in an ultrasonic bath.

2.1.2. Characterization of the particles

Particle imaging was performed using scanning electron microscopy (Jeol JSM-6010LA), white light interferometry (Bruker) and 3D optical microscopy (Keyence).

2.1.3. Release of the particle

A 40 μL water droplet was placed on the printed structures to release the particles in an aqueous dispersion and a second coverslip was attached by means of a double-sided tape to seal the system and prevent evaporation (Fig. 1e). The dimensions of the liquid cell were 0.9*1.5 cm with a thickness of 120 μm. The particles were released by dissolving the PVA layer with a 10 s immersion in an ultrasonic bath (Fig. 1f).

2.1.4. Imaging

The motion of the colloidal particles was recorded using an inverted microscope (Nikon Eclipse Ti-E equipped with a Zyla camera in the fluorescent (FITC)[8] mode). Movies were recorded at the rate of 40 frames per second with an exposure time of 20 ms to minimize the dynamic error [58].

2.2. Video microscopy analysis

The RGB images were converted into grayscale format and their contrast was improved. The adjusted grayscale images were binarized based on a threshold. This threshold was chosen such that particle features were clearly visible, and they retained their original shape and size. Once the image was binarized, the leftover salt-and-pepper noise was eliminated using a median filter. The external boundaries of the particles were traced based on the Moore-neighbour tracing algorithm modified by Jacob's stopping criteria [59]. The same method can be used to trace the internal

[8] FITC – Fluorescent.

Table 3-1
Dimensions of disk shaped particles with circular cross-section (r - Particle radius, h - Particle thickness).

Type		2r (μm)	h (μm)
Circular	C1	1	1
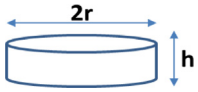	C3	3	1
	C5	5	1
	C10	10	1

boundaries in the object however, since there were no holes or patterns in the particles of interest, internal boundaries were not traced. Once all the desired particles were identified, their centroid was estimated. It was assumed that the particles had uniform density and so the centroid of a particle was same as its centre of mass. The centre of mass of a particle served as its location in an image. A position list was generated to tabulate the location (X-Y centroid) of the identified particles in successive images. A trajectory was generated, based on the algorithm developed by Crocker and Grier [60], by tracking the centre of mass of the objects over the subsequent images. The trajectory was then used to calculate the MSD of the objects over different lag times.

The slope of the MSD vs lag time curve was used to calculate of the in-plane diffusion coefficient of the particle.

$$MSD = 4Dt$$

where MSD is the mean squared displacement, D is the diffusion coefficient and t is the lag time.

It is important to note that the as the lag time increases the number of particle displacements decreases and this consequently increases the statistical uncertainty. Hence, slope is estimated based on the points for which the statistical uncertainty is less than 2%.

3. Results & discussion

3.1. Optimization of the colloidal particle fabrication

In this paper, two photon polymerization was used to fabricate colloidal particles with custom shape geometry. We selected 3 particle geometries for analysis (circular, rectangular and triangular) with dimensions ranging from 1 μm to 10 μm. All the geometries and dimensions are listed in Table 3-1–3-3.

The first step in the production of colloidal particles via 2-photon polymerization is the design of the 3D shape using the CAD software. This CAD model is then sliced horizontally, and each slice is divided into lines as shown in Table 3-4. The slicing distance corresponds to the thickness of each printed layer. The hatching distance corresponds to the width of each line. This is the way the particles are also produced by the 2PP printer. In fact, the movement of the laser follows the lines and layer by layer (one slice after the other) builds the 3D object. Ideally the slicing and hatching distance are tuned in such a way to produce a solid object. This means that the lines printed sequentially are touching each other both in XY and Z direction. If those distances are too high, adjacent lines and/or slices (or layers) cannot bond together and are not connected, thereby losing the integrity of the printed object.

As previously mentioned, the laser used for 2PP is an infrared laser. One important parameter is the tuning of the laser power (Laser Power Output [mW] = Laser Power [%] × (Power Scaling × 50 [mW]) / 100). This is tightly coupled with the scan speed, which is the speed at which the laser moves to produce the object. Usually the faster the printing; the higher the laser power required. In fact, the 2PA process has an energy threshold above which the polymerization of the uncured (liquid) resin starts. The laser dose needs to be high enough to overcome this threshold.

To produce particles via 2PP, it is necessary to optimize all the parameters that have been described: slicing and hatching distance, laser power and scan speed. For this reason, we printed a matrix for each particle geometry and dimension and examined the effect of the printing parameters described above (see Supplementary information). If the slicing and hatching distance were small and the laser power was high (high dose) the polymer started to boil, and the printed structures were deformed. On the other hand, if the slicing and hatching distance were small and the laser power was low (low dose), then the presence of a threshold energy prevented polymerization and consequently the particles were not printed. The optimal parameters, listed in Table 3-4, were chosen to maximize the printing accuracy with respect to the original CAD design for each particle dimension.

We observed that the shape of the particle did not influence the printing parameters. This may be because the printing process was independent of the particle geometry. However, the parameters depend on the particle dimension due to the higher resolution required for smaller particles. This is reflected in the need of reducing the hatching and slicing distance, which directly improves the printing quality, allowing fabrication of small particles.

Fig. 2a, b, c shows the images of typical printed particles acquired using scanning electron microscopy (SEM). Particles of those types were used in the tracking experiment. Other images of the particles can be found in the Supplementary Information.

Table 3–2
Dimensions of particles with triangular cross-section (L - Base of the triangle, H – Lateral height, h - Particle thickness).

Type		L (μm)	H (μm)	h (μm)
Triangular	T1	1	1	1
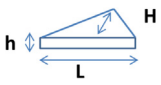	T3	3	3	1
	T5	5	5	1
	T10	10	10	1

Table 3–3
Dimensions of particles with rectangular cross-section (L1 – Particle breadth, L2 – Particle length, h – Particle thickness).

Type		L1 (μm)	L2 (μm)	h (μm)
Rectangular	R1	1	2	1
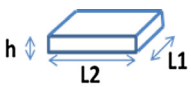	*R*3	3	6	1
	R5	5	10	1
	R10	10	20	1

Table 3–4
List of all optimized parameters for fabrication of particles using 2PP.

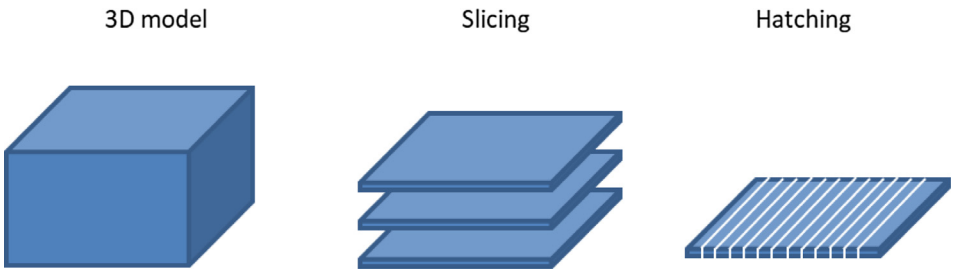

Particle type	Laser power (%)	Scan speed (μm/s)	Slicing distance (μm)	Hatching distance (μm)
C1, R1, T1	40	10,000	0.05	0.07
C3, R3, T3	50	20,000	0.1	0.07
C5, R5, T5	50	30,000	0.1	0.1
C10, R10, T10	50	30,000	0.1	0.1

3D optical images were acquired, using a white-light interferometer, to evaluate the lateral dimension and the thickness of the particles (see Supplementary information). The dimensions of the printed particles matched the design dimensions with a printing accuracy of ±10–15% defined as the difference between the printed dimension, d_{print} and the design dimension, d_{design} normalized by d_{design}. Fig. 2e, f, g shows the comparison between the CAD design and the printed dimension for each type of particle. The line represents the 1:1 match. The error bars for determining the particle dimensions are based on repeating the experiment at least three times and the standard deviation is given as error bar. All the points with error bars lie on the line demonstrating the high accuracy of the printing process in producing custom designed features up to a minimum dimension of 1 μm. The thickness of the particles was 1 μm (±4%).

Since the particles are printed one at the time, the printing time can be very long depending on the chosen printing parameters. For instance, it was observed that decreasing the slicing distance or the hatching distance, increased the printing time. By using the optimal printing parameters based on the highest printing accuracy, it was possible to produce up to 4000 particles (disk of 1 μm diameter and height, C1) in one hour (for other particle dimensions see supplementary information). Compared to lithographic techniques producing as many as 180 million particles in one iteration leveraging clean room equipment (stepper, mask aligner) [40], the number of particles produced in 2PP is not very high (~4000/h). However, this comparison does not take into account the flexibility and automation 2PP offers for the realization of custom 3D shapes. Moreover, 2PP can operate automatically repeating particle fabrication continuously once the process parameters are optimized. So, in conclusion, the lower yield of the 2PP process is compensated by the flexibility it offers in defining the particle geometry and automated operation. We present 2PP technique as a complementary approach to the lithographic ones with distinct advantages in flexibility and operation.

Once printing was completed and the uncured resin was removed, the sample was dried. It was observed that the particles adhered to the PVA layer and the sample could be stored for at least 1 month in a dry environment. This permitted convenient handling of the particles. Sacrificial layer of PVA can be dissolved in water enabling the release of colloidal particles produced via 2PP. PVA is a water-soluble polymer commonly used in microfabrication, hence PVA was chosen as the sacrificial layer. It is crucial to avoid the use of solvents that may affect the shape of the printed particles. We found no evident shrinkage of the particles in water.

3.2. Particle Brownian motion

Colloidal particles exhibit random walk when suspended in a Newtonian fluid, for example in water. One way to characterize this motion is by estimating the mean squared displacement ($<r^2>$)[9] of the particles. The particle trajectories are used to calculate their MSD as shown in Eq. (3.1).

$$< r^2(\tau) >=< ((r(t+\tau) - r(t))^2 > \quad (3.1)$$

The mean squared displacement (MSD) of the particles diffusing in a plane (2D) increases linearly with lag time (τ)[10].

$$< r^2(\tau) >= 4D_i\tau \quad (3.2)$$

where D_i[11] is the translational diffusion coefficient in bulk ($i = \infty$) or close to the surface ($i = 0$).

A 40 μL water droplet was placed on the printed structures and a second coverslip was attached by means of a double-sided tape in order to seal the system and prevent evaporation. The particles were released from the surface by sonicating the sample for 10 s in an ultrasonic bath, consequently dissolving the PVA layer. The Brownian motion of the auto-fluorescent particles was captured in the fluorescence mode using video microscopy (see supplementary information). Images were taken at a distance of at least 15 μm from the surface of the bottom glass slide.

The MSD is plotted as a function of the lag times in Fig. 3a, b, c for circular, rectangular and triangular particles respectively. The MSD reported in Fig. 3 is the arithmetic mean of mean square displacements in x and y directions. We observed slight deviation (2–8%) between MSD values in x and y directions. A larger deviation (15–30%) is observed for 10 μm particles. We attribute observed deviations to non-systematic drift and imperfections in particle geometry. The static error was estimated (see Supplementary information) by measuring the MSD of the printed particles stuck to the glass slide and not released in water.

A linear fit of the graphs in Fig. 3a, b, c, using Eq. (3.2), provides an estimate of the diffusion coefficient for each particle dimension and shape ($R^2 - 0.99$). The experiment to determine diffusion coefficient was performed only once yet at least 2000 time lag points were used for each particle. The result is shown in Fig. 3d where the diffusion coefficient is plotted in function of the volume of the particle. As expected, the diffusion coefficient decreased as the particle volume increased.

[9] Mean squared displacement.
[10] Lag time.
[11] Translational diffusion coefficient at position i.

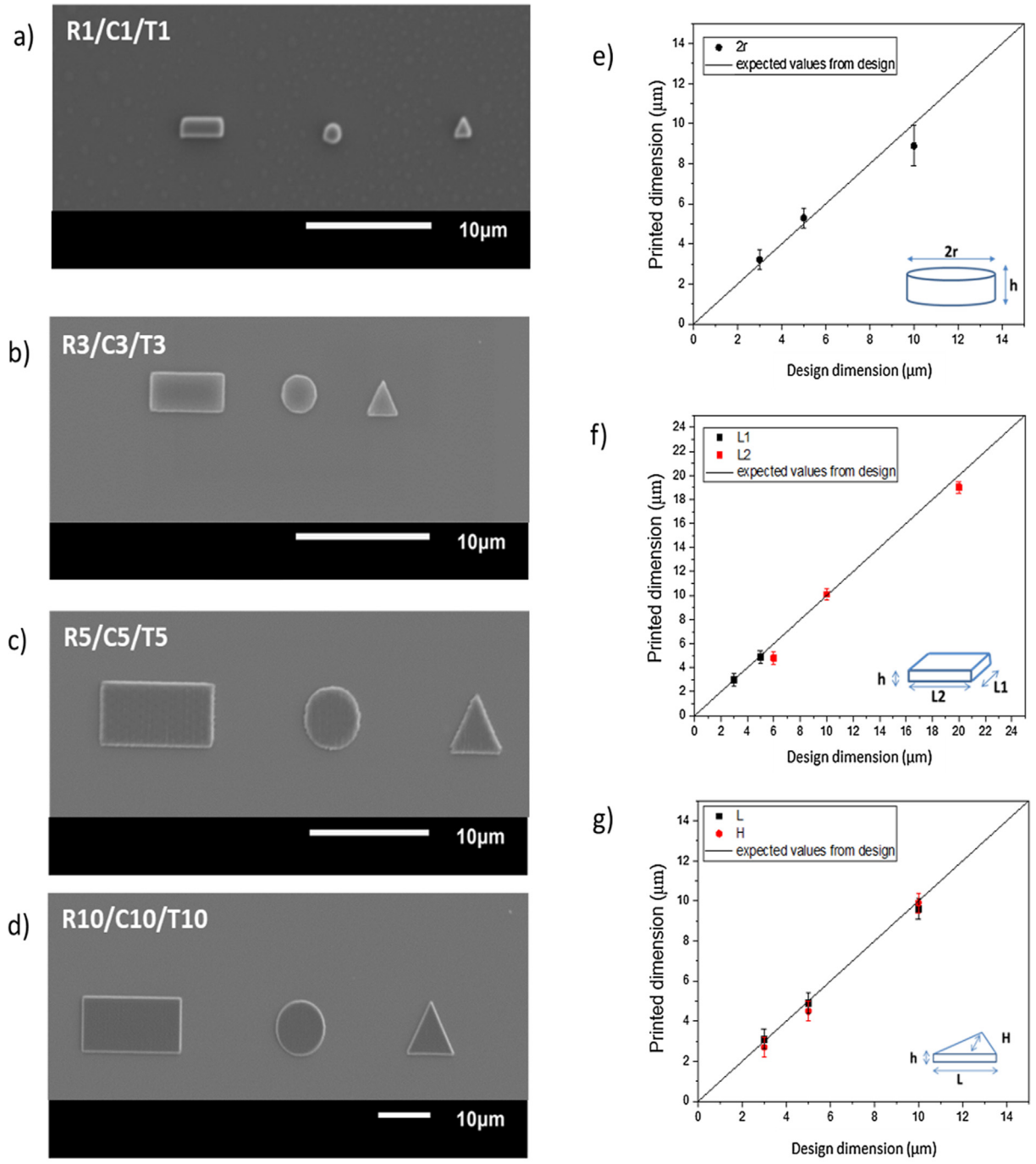

Fig. 2. Optimization of 2PP polymerization: Scanning electron microscope images of printed particles of (a) 1 µm (b) 3 µm (c) 5 µm (d) 10 µm. Comparison between the CAD design dimension and the printed dimension measured from SEM images for particles with (e) circular shape (f) rectangular shape (g) triangular shape.

The translational diffusion coefficient of a sphere (D_{sph}[12]) is dependent on its radius (r_{sph}[13]), by the Stokes-Einstein-Sutherland equation [61] as shown in Eq. (3.3).

$$D_{sph} = \frac{kT}{6\pi\eta r_{sph}} \tag{3.3}$$

where,

k – Boltzmann constant

T – Temperature of the fluid

η – fluid viscosity

For thin circular disks, the diffusion coefficient is a function of its aspect ratio[14] (p), which is defined as

$$p = \frac{h}{2r} \tag{3.4}$$

where,

h – height of the circular disk

r – radius of the circular disk

[12] Translational diffusion coefficient of sphere.

[13] Radius of sphere.

[14] Particle aspect ratio.

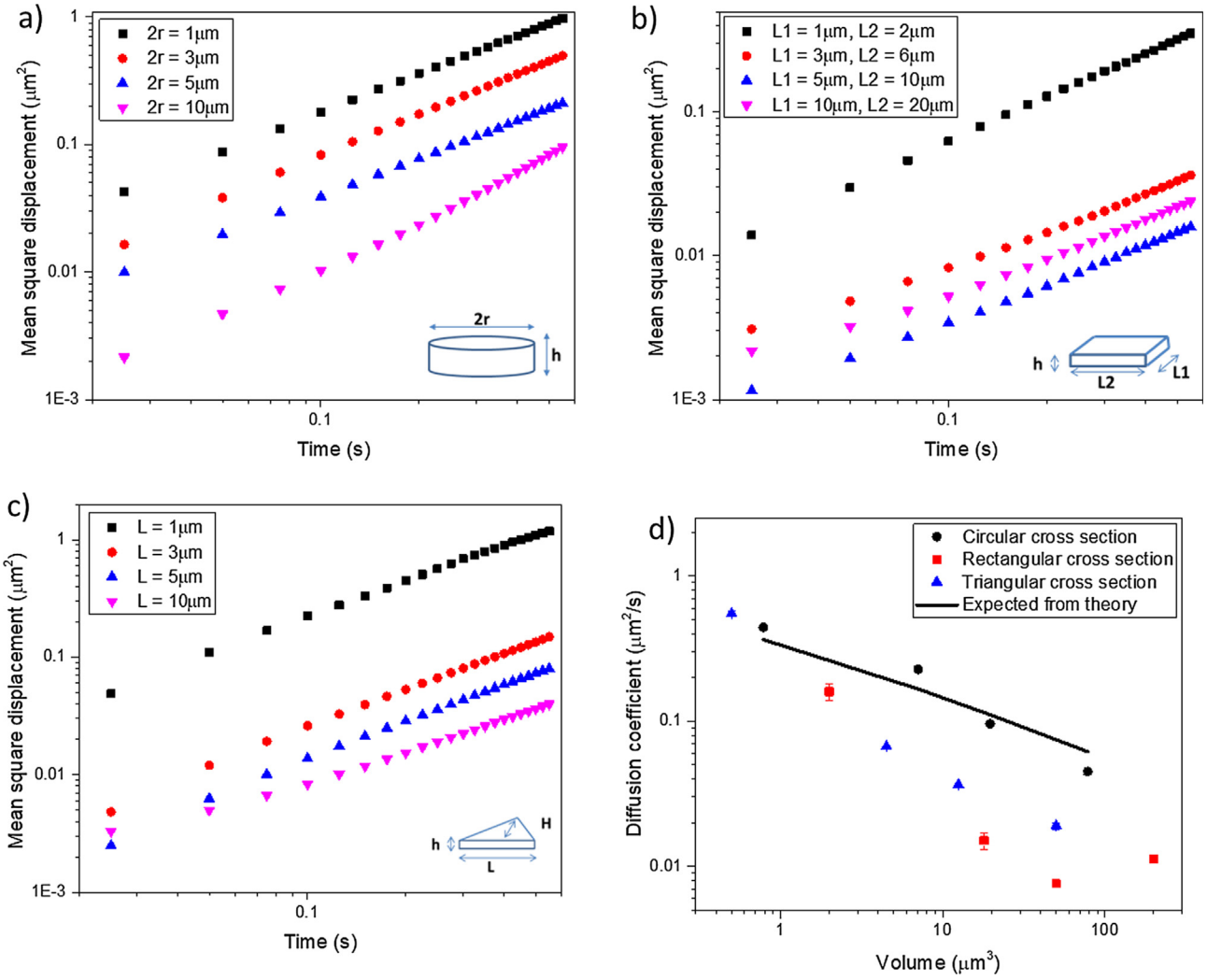

Fig. 3. MSD plotted as a function of the lag time for different dimensions of the particles with (a) circular cross section (b) rectangular cross section (c) triangular cross section (d) Diffusion coefficient is plotted in function of particle volume.

An empirical model, developed by Hansen [62] was used to predict the diffusion coefficient of the disk shaped particles. The model is based on Monte Carlo simulations and provides a correlation between the bulk diffusivity, D_∞[15] and the aspect ratio p.[16]

$$\frac{D_s}{D_\infty} = 1.0304 + 0.0193\ln p + 0.0623(\ln p)^2 + 0.048(\ln p)^3 + 0.0017(\ln p)^4 \quad (3.5)$$

where D_s[17] is the bulk diffusion coefficient of a sphere with the same volume as the disk.

The model in Eq. (3.5) denoted by the solid line in Fig. 3d fits well with the measured diffusion coefficient (±9–13%) of the disk particles with a given aspect ratio. However, a significant deviation is observed for triangular and rectangular particles. This was expected due to the coupling between the particle shape and hydrodynamics. A second significant deviation from expectations appears for rectangular particles. The largest rectangular particle (L1 = 10 μm, L2 = 20 μm) shows faster dynamics than the second largest rectangular particle (L1 = 5 μm, L2 = 10 μm). This is unexpected. We attribute this discrepancy to uncertainty in determining observation height and drift introduced due to a change in experimental procedure for these particles. The largest rectangular particles sediment considerably faster than other particles inside the chamber. In order to get good statistics, these experiments were repeated by turning the glass chamber upside down. Each time the glass slide was turned, the observation depth was readjusted. This leads to human error in determining the observation height. Moreover, we believe turning the glass chamber upside down gave rise to convection currents within the glass chamber. These convection currents might have introduced drift, thereby artificially increasing the measured diffusion coefficient. Another issue that is worth addressing is the potential water adsorption by 2PP particles. As these particles are crosslinked polymer networks, water adsorption can lead to swelling and increase in their size. If this was a significant effect, the theoretical prediction for disks to be consistently above the experimental values. This is not the case. Consequently, we conclude that swelling might occur however it is not the most pronounced effect explaining the deviation observed in Fig. 3d. Although, the development of an analytical model, which describes the diffusion behaviour of complex particle geometries, is beyond the scope of this paper, our study

[15] Bulk diffusivity.
[16] Particle aspect ratio.
[17] Bulk diffusivity of sphere with same volume as volume of disk.

demonstrates that the detailed geometry must be taken into account while considering the diffusion of shape anisotropic particles [63].

An experimental issue worth discussing is the influence of poly (vinly alchol) that remains in solution upon release of particles. The residual PVA can influence the Brownian motion of particles either by increasing the viscosity of solution, or by increasing the hydrodynamic radius by adsorption. Given the cell dimensions, PVA layer thickness and assuming all the PVA dissolves in water, we estimate the weight fraction of PVA as 0.04% or 0.004 g/dL. At this weight fraction, residual PVA cannot change the viscosity of the water significantly [67]. PVA adsorption is a more likely scenario as PVA is commonly used as a stabilizing agent for various colloidal systems. The radius of gyration of PVA dissolved in water at the molecular weight used in this study has been measured as approximately 2–3 nm [66]. Even if we assume that adsorbed PVA increases the dimensions of colloids by its radius of gyration, the smallest dimension will not be increased more than 0.3%. This value is well within our accuracy for calculating diffusion coefficients.

The shape dependent diffusion coefficients dictate the time scale for self-assembly. For instance, a self-assembled structure can be kinetically arrested if the time scale associated with its formation is significantly larger than experimental time scale [64]. In essence, measuring the diffusion coefficient at low concentrations (ϕ[18] < 0.1%) allows us to test theoretical predictions from finite element simulations based on calculating the hydrodynamic drag and resistance tensor [65–67]. Our results contribute to the experimental literature [63] to test simulation results [64].

Moreover, how the shape influences the interparticle hydrodynamic coupling and consequently the diffusion coefficient at moderate and high concentrations (0.1 < ϕ < 10%) (ϕ > 10%) is still a topic attracting wider interest, for instance, in rheological flows of concentrated suspensions essential in material manufacturing and multi-phase flows. Our 2PP technique can contribute to addressing critical questions in these fields.

4. Conclusions and recommendations

In conclusion, shape anisotropic colloidal particles were fabricated by 2-photon polymerization, an additive manufacturing technique [48,51,54–56]. The process was optimized to obtain high printing accuracy i.e. minimum deviation of the printed dimensions from the CAD design (±10–15%) for in-plane and out-of plane dimensions. Particles with rectangular, triangular and circular geometries were produced down to a minimum dimension of 1 μm. We demonstrated that the fabricated particles can be easily released by dissolving the sacrificial PVA layer in water and their motion can be tracked to generate particle trajectories by video microscopy [60]. The particle trajectories were used to estimate their diffusion coefficient in aqueous medium. The diffusion coefficient of disk shaped particles fitted well with the values predicted using existing models [62]. However, increased anisotropy, in rectangular and triangular geometries, led to pronounced deviation from the predicted values. This deviation is attributed to stronger hydrodynamic coupling between the particle shape and the surrounding fluid with increasing anisotropy [63]. The observed deviation emphasizes the relevance of particle geometry on accurately predicting diffusion coefficient. Our study highlights 2PP as a complementary method for manufacturing colloidal building blocks. Currently, it has limited yield (4000 particle per hour for disks of 1 μm diameter and height) compared to wet-chemistry [25–27] and lithographic methods [40–43]. However, 2PP can be used with limited knowledge of colloidal chemistry and it does not require access to cleanrooms equipment. Moreover, it offers automated operation and easy alterations in particle geometry with CAD software. We believe the design flexibility, automated nature, printing accuracy, convenient handling of the sample and easy up-scalability of the 2PP fabrication of colloidal building blocks will open new alleys of investigation in colloid science [3,68], drug delivery [18,21], bottom-up tissue engineering [55], diagnostics [17] and beyond.

[18] Particle volume fraction.

CRediT authorship contribution statement

Burak Eral, Luigi Sasso: Conceptualization; **Paola Fanzio, Yug Saraswat:** Data curation; **Paola Fanzio, Yug Saraswat:** Formal analysis; **Burak Eral, Luigi Sasso:** Funding acquisition; **Paola Fanzio, Burak Eral, Luigi Sasso, Yug Saraswat, Fatma Ibis, Laura Rossi:** Investigation; **Paola Fanzio, Burak Eral, Yug Saraswat, Fatma Ibis:** Methodology; **Burak Eral, Luigi Sasso, Fatma Ibis:** Project administration; **Burak Eral, Paola Fanzio, Luigi Sasso:** Resources; **Burak Eral, Paola Fanzio:** Software; **Burak Eral, Luigi Sasso, Fatma Ibis:** Supervision; **Burak Eral, Paola Fanzio, Yug Saraswat:** Validation; **Burak Eral, Paola Fanzio, Yug Saraswat:** Visualization; **Yug Saraswat, Paola Fanzio, Burak Eral:** Writing - Original draft; **Yug Saraswat, Burak Eral, Paola Fanzio, Luigi Sasso, Laura Rossi:** Writing - review & editing.

Acknowledgments

Authors would like to thank Rob Luttjeboer for his valuable help in 2PP. H.B.E and L.R. acknowledge the Netherlands Organisation for Scientific Research (NWO), Netherlands for financial support through Veni grants (project numbers 722-014-007 and 680-47-446).

Appendix A. Supplementary material

Supplementary data to this article can be found online at https://doi.org/10.1016/j.jcis.2019.12.035.

References

[1] L. Onsager, The effects of shape on the interaction of colloidal particles, Ann. N. Y. Acad. Sci. 51 (4) (1949) 627–659.
[2] W.E. Uspal, H.B. Eral, P.S. Doyle, Engineering particle trajectories in microfluidic flows using particle shape, Nat. Commun. 4 (2013) 2666.
[3] S.C. Glotzer, Nanotechnology: shape matters, Nature 481 (7382) (2012) 450.
[4] É. Ducrot et al., Colloidal alloys with preassembled clusters and spheres, Nat. Mater. 16 (6) (2017) 652.
[5] L. Rossi et al., Shape-sensitive crystallization in colloidal superball fluids, Proc. Natl. Acad. Sci. 112 (17) (2015) 5286–5290.
[6] P.F. Damasceno, M. Engel, S.C. Glotzer, Predictive self-assembly of polyhedra into complex structures, Science 337 (6093) (2012) 453–457.
[7] S.H. Lee et al., Synthesis and assembly of nonspherical hollow silica colloids under confinement, J. Mater. Chem. 18 (41) (2008) 4912–4916.
[8] S. Sacanna et al., Lock and key colloids, Nature 464 (7288) (2010) 575.
[9] C. Kang, A. Honciuc, Influence of Geometries on the Assembly of Snowman-Shaped Janus Nanoparticles, ACS nano 12 (4) (2018) 3741–3750.
[10] Rehor, I., et al., Biodegradable microparticles for simultaneous detection of counterfeit and deteriorated edible products. Small 13(39) (2017) 1701804.
[11] T.D. Nguyen, E. Jankowski, S.C. Glotzer, Self-assembly and reconfigurability of shape-shifting particles, ACS nano 5 (11) (2011) 8892–8903.
[12] J.D. Forster et al., Assembly of optical-scale dumbbells into dense photonic crystals, ACS nano 5 (8) (2011) 6695–6700.
[13] C.X. Du et al., Shape-driven solid–solid transitions in colloids, Proc. Natl. Acad. Sci. 114 (20) (2017) E3892–E3899.
[14] O. Gang, Y. Zhang, Shaping phases by phasing shapes, ACS nano 5 (11) (2011) 8459–8465.
[15] T. Ding et al., Fabrication of 3D photonic crystals of ellipsoids: convective self-assembly in magnetic field, Adv. Mater. 21 (19) (2009) 1936–1940.
[16] N. Doshi, et al., Red blood cell-mimicking synthetic biomaterial particles, in: Proceedings of the National Academy of Sciences, 2009: p. pnas. 0907127106.

[17] L.C. Glangchai et al., Nanoimprint lithography based fabrication of shape-specific, enzymatically-triggered smart nanoparticles, J. Control. Release 125 (3) (2008) 263–272.
[18] S. Bhaskar et al., Towards designer microparticles: simultaneous control of anisotropy, shape, and size, Small 6 (3) (2010) 404–411.
[19] S.H. Im, U. Jeong, Y. Xia, Polymer hollow particles with controllable holes in their surfaces, Nat. Mater. 4 (9) (2005) 671.
[20] J.A. Champion, Y.K. Katare, S. Mitragotri, Particle shape: a new design parameter for micro-and nanoscale drug delivery carriers, J. Control. Release 121 (1–2) (2007) 3–9.
[21] S. Mitragotri, In drug delivery, shape does matter, Springer, 2009.
[22] H.Z. An et al., Synthesis of colloidal microgels using oxygen-controlled flow lithography, Soft Matter 10 (38) (2014) 7595–7605.
[23] S. Sacanna, D.J. Pine, G.-R. Yi, Engineering shape: the novel geometries of colloidal self-assembly, Soft Matter 9 (34) (2013) 8096–8106.
[24] C.H. Choi et al., Surface-tension-induced synthesis of complex particles using confined polymeric fluids, Angewandte Chemie International Edition 49 (42) (2010) 7748–7752.
[25] A. Kuijk, A. van Blaaderen, A. Imhof, Synthesis of monodisperse, rodlike silica colloids with tunable aspect ratio, JACS 133 (8) (2011) 2346–2349.
[26] J. Zhang, et al., Au-induced polyvinylpyrrolidone aggregates with bound water for the highly shape-selective synthesis of silica nanostructures, Chem. – A Eur. J. 14(14) (2008) 4374–80.
[27] J. He et al., Wet-chemical synthesis of amphiphilic rodlike silica particles and their molecular mimetic assembly in selective solvents, Angewandte Chemie International Edition 51 (15) (2012) 3628–3633.
[28] I. Lesov et al., Bottom-up synthesis of polymeric micro-and nanoparticles with regular anisotropic shapes, Macromolecules 51 (19) (2018) 7456–7462.
[29] J.P. Rolland et al., Direct fabrication and harvesting of monodisperse, shape-specific nanobiomaterials, JACS 127 (28) (2005) 10096–10100.
[30] S. Sacanna et al., Fluorescent monodisperse silica ellipsoids for optical rotational diffusion studies, Langmuir 22 (4) (2006) 1822–1827.
[31] S. Hou, J. Wang, C.R. Martin, Template-synthesized DNA nanotubes, JACS 127 (24) (2005) 8586–8587.
[32] J.L. Perry et al., PRINT: a novel platform toward shape and size specific nanoparticle theranostics, Acc. Chem. Res. 44 (10) (2011) 990–998.
[33] S. Sacanna et al., Shaping colloids for self-assembly, Nat. Commun. 4 (2013) 1688.
[34] T. Van Dillen et al., Ion beam-induced anisotropic plastic deformation at 300 keV, Appl. Phys. Lett. 83 (21) (2003) 4315–4317.
[35] K.P. Velikov et al., Photonic crystals of shape-anisotropic colloidal particles, Appl. Phys. Lett. 81 (5) (2002) 838–840.
[36] J.-G. Park, J.D. Forster, E.R. Dufresne, Synthesis of colloidal particles with the symmetry of water molecules, Langmuir 25 (16) (2009) 8903–8906.
[37] J.W. Kim, R.J. Larsen, D.A. Weitz, Uniform nonspherical colloidal particles with tunable shapes, Adv. Mater. 19 (15) (2007) 2005–2009.
[38] J.-W. Kim, R.J. Larsen, D.A. Weitz, Synthesis of nonspherical colloidal particles with anisotropic properties, JACS 128 (44) (2006) 14374–14377.
[39] J.A. Champion, Y.K. Katare, S. Mitragotri, Making polymeric micro-and nanoparticles of complex shapes, Proc. Natl. Acad. Sci. 104 (29) (2007) 11901–11904.
[40] C.J. Hernandez, T.G. Mason, Colloidal alphabet soup: monodisperse dispersions of shape-designed lithoparticles, J. Phys. Chem. C 111 (12) (2007) 4477–4480.
[41] S. Badaire et al., Shape selectivity in the assembly of lithographically designed colloidal particles, JACS 129 (1) (2007) 40–41.
[42] J.H. Moon et al., High-throughput synthesis of anisotropic colloids via holographic lithography, Adv. Mater. 19 (18) (2007) 2508–2512.
[43] J.-H. Jang et al., Shape control of multivalent 3D colloidal particles via interference lithography, NANO Lett. 7 (3) (2007) 647–651.
[44] D. Dendukuri, P.S. Doyle, The synthesis and assembly of polymeric microparticles using microfluidics, Adv. Mater. 21 (41) (2009) 4071–4086.
[45] D. Dendukuri et al., Stop-flow lithography in a microfluidic device, Lab Chip 7 (7) (2007) 818–828.
[46] J.I. Park et al., Microfluidic synthesis of polymer and inorganic particulate materials, Annu. Rev. Mater. Res. 40 (2010) 415–443.
[47] H.C. Shum et al., Droplet microfluidics for fabrication of non-spherical particles, Macromol. Rapid Commun. 31 (2) (2010) 108–118.
[48] B. Bhushan, M. Caspers, An overview of additive manufacturing (3D printing) for microfabrication, Microsyst. Technol. 23 (4) (2017) 1117–1124.
[49] I. Zein et al., Fused deposition modeling of novel scaffold architectures for tissue engineering applications, Biomaterials 23 (4) (2002) 1169–1185.
[50] A. Bertsch, H. Lorenz, P. Renaud, 3D microfabrication by combining microstereolithography and thick resist UV lithography, Sens. Actuat. A 73 (1–2) (1999) 14–23.
[51] K.S. Lee et al., Recent developments in the use of two-photon polymerization in precise 2D and 3D microfabrications, Polym. Adv. Technol. 17 (2) (2006) 72–82.
[52] S. Wu, J. Serbin, M. Gu, Two-photon polymerisation for three-dimensional micro-fabrication, J. Photochem. Photobiol., A 181 (1) (2006) 1–11.
[53] J. Serbin et al., Femtosecond laser-induced two-photon polymerization of inorganic–organic hybrid materials for applications in photonics, Opt. Lett. 28 (5) (2003) 301–303.
[54] A. Ovsianikov et al., Two-photon polymerization of hybrid sol-gel materials for photonics applications, Laser Chem. 2008 (2008).
[55] A. Ovsianikov et al., Two-photon polymerization technique for microfabrication of CAD-designed 3D scaffolds from commercially available photosensitive materials, J. Tissue Eng. Regener. Med. 1 (6) (2007) 443–449.
[56] D. Wu et al., Femtosecond laser rapid prototyping of nanoshells and suspending components towards microfluidic devices, Lab Chip 9 (16) (2009) 2391–2394.
[57] S. Kawata et al., Finer features for functional microdevices, Nature 412 (6848) (2001) 697.
[58] T. Savin, P.S. Doyle, Static and dynamic errors in particle tracking microrheology, Biophys. J . 88 (1) (2005) 623–638.
[59] R.C. Gonzalez, R.E. Woods, S. Eddins, Digital Image Processing Using MATLAB: Pearson Prentice Hall, Upper Saddle River, New Jersey, 2004.
[60] J.C. Crocker, D.G. Grier, Methods of digital video microscopy for colloidal studies, J. Colloid Interface Sci. 179 (1) (1996) 298–310.
[61] J.T. Edward, Molecular volumes and the Stokes-Einstein equation, J. Chem. Educ. 47 (4) (1970) 261.
[62] S. Hansen, Translational friction coefficients for cylinders of arbitrary axial ratios estimated by Monte Carlo simulation, J. Chem. Phys. 121 (18) (2004) 9111–9115.
[63] H. Eral et al., Anisotropic and hindered diffusion of colloidal particles in a closed cylinder, Langmuir 26 (22) (2010) 16722–16729.
[64] H. Eral, F. Mugele, M.H. Duits, Colloidal dynamics near a particle-covered surface, Langmuir 27 (20) (2011) 12297–12303.
[65] B. Bet et al., Calculating the motion of highly confined, arbitrary-shaped particles in Hele-Shaw channels, Microfluidics and nanofluidics 22 (8) (2018) 77.
[66] B. Bet et al., Steering particles by breaking symmetries, J. Phys.: Condens. Matter 30 (22) (2018) 224002.
[67] T. Beatus et al., Two-dimensional flow of driven particles: a microfluidic pathway to the non-equilibrium frontier, Chem. Soc. Rev. 46 (18) (2017) 5620–5646.
[68] T.G. Anjali, M.G. Basavaraj, Shape-Anisotropic Colloids at Interfaces, Langmuir 35 (1) (2019) 3–20.